THE JOURNAL OF PHYSICAL CHEMISTRY Letters

Letter

pubs.acs.org/JPCL

Resolving the Iron Phthalocyanine Redox Transitions for ORR Catalysis in Aqueous Media

Amell Alsudairi,[†,‡] Jingkun Li,[†] Nagappan Ramaswamy,[†,§] Sanjeev Mukerjee,[†] K. M. Abraham,[†] and Qingying Jia*[,†]

[†]Department of Chemistry and Chemical Biology, Northeastern University, Boston, Massachusetts 02115, United States

[‡]Chemistry Department, Faculty of Science, King Abdulaziz University, P.O. Box 80200, Jeddah 21589, Saudi Arabia

Supporting Information

ABSTRACT: Metal macrocycles are among the most important catalytic systems in electrocatalysis and biocatalysis owing to their rich redox chemistry. Precise understanding of the redox behavior of metal macrocycles in operando is essential for fundamental studies and practical applications of this catalytic system. Here we present electrochemical data for the representative iron phthalocyanine (FePc) in both aqueous and nonaqueous media coupled with in situ Raman and X-ray absorption analyses to challenge the traditional notion of the redox transition of FePc at the low potential end in aqueous media by showing that it arises from the redox transition of the ring. Our data unequivocally demonstrate that the electron is shuttled to the Pc ring via the Fe(II)/Fe(I) redox center. The Fe(II)/Fe(I) redox transition of FePc in aqueous media is indiscernible by normal spectroscopic methods owing to the lack of a suitable axial ligand to stabilize the Fe(I) state.

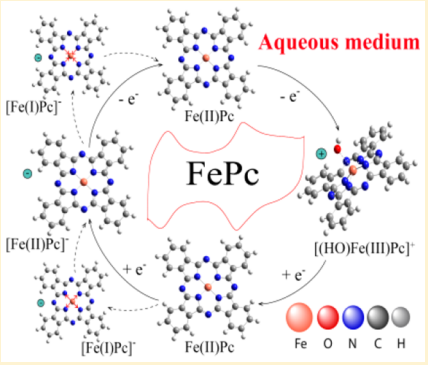

The biomimetic metal macrocycle-based materials are the frontrunners as nonprecious metal catalysts for the oxygen reduction reaction (ORR) in proton exchange membrane fuel cells,[1−8] chemically regenerative redox fuel cells,[9] alkaline anion exchange membrane fuel cells,[9,10] and Li−air batteries.[11−13] The high catalytic activity of this class of materials arises largely from its rich redox chemistry associated with the unique structure of the transition-metal ions coordinated by nitrogen-based macrocycle rings. Despite the small structural variations within metal macrocycles, the role of the metal center in ORR catalysis is well recognized.[10,14−16] It is generally believed that the ORR is mediated by the M−N_4 center via the redox transition of the central metal in aqueous media; and the redox potential is the primary activity descriptor for the ORR activity of M−N_4 moieties.[3,17−20] The differences in the ORR kinetics and activity of M−N_4 moieties in acid and alkaline media are primarily induced by the redox potential shift with pH values[17,21] and the different key intermediates (H_2O_2 vs HO_2^-).[21] Contemporarily, our previous study[12] showed that cobalt phthalocyanine (CoPc) exhibits a decent ORR activity in the nonaqueous environment of the Li−air battery due to the stabilization of O_2^- on the Co−N_4 site. We later extended the work to Fe−N_4 moieties and showed that the ORR is catalyzed by the Fe(II)/Fe(I) redox transition with Fe(I)−N_4 being the active site.[13] This differs from the case in aqueous media in which the ORR is catalyzed by the Fe(III)/Fe(II) redox transition, with Fe(II)−N_4 being the active site.[18] While the key roles of the redox transition of M−N_4 moieties in mediating ORR have been recognized,[3,17,18] the associated redox chemistry remains largely vague. Numerous metal macrocycles such as the iron phthalocyanine (FePc) exhibit two redox peaks in both acid (Figure 1) and alkaline media (Figure S1).[22,23] It is clear that the redox peaks at the higher potential are associated with the Fe(III)/Fe(II) redox transition, but those at the lower potential are inconclusive. Whereas the majority of researchers

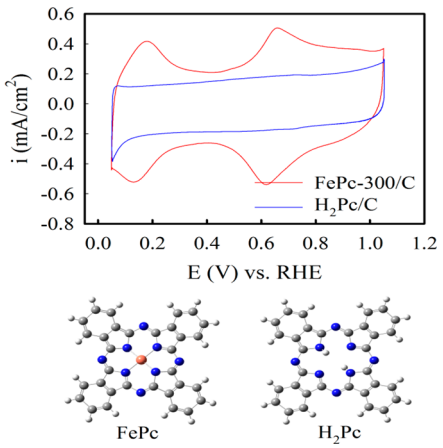

Figure 1. Cyclic voltammogram (CV) plots of FePc-300/C and H_2Pc/C (structures illustrated) in an Ar-saturated 0.1 M $HClO_4$ electrolyte at 20 mVs^{-1}. The FePc/C was subjected to 300 °C (denoted as FePc-300/C) to tightly anchor FePc onto the carbon substrate without altering its local structure,[3,13] necessary for the long-term in situ X-ray absorption spectroscopy (XAS) characterization.

Received: May 8, 2017
Accepted: June 9, 2017
Published: June 9, 2017

DOI: 10.1021/acs.jpclett.7b01126
J. Phys. Chem. Lett. 2017, 8, 2881−2886

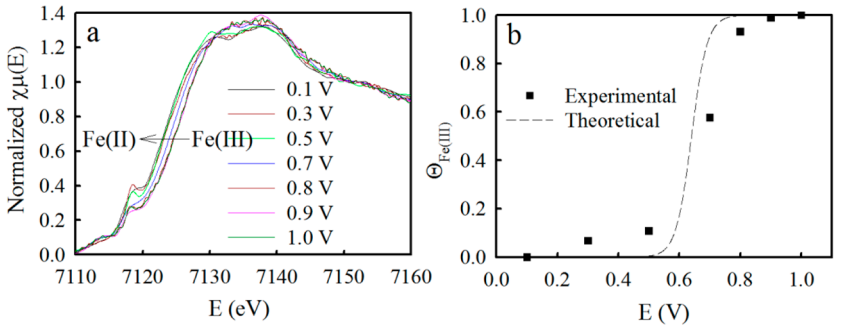

Figure 2. (a) In situ XANES of FePc-300/C collected at 0.1 to 1.0 V_{RHE} in N_2-saturated 0.1 M $HClO_4$. (b) Experimental $\Theta_{Fe(III)}$ for FePc-300/C, in comparison with the calculated $\Theta_{Fe(III)}$ derived from eq 2.

assigned these to the Fe(II)/Fe(I) redox transition,[22−24] a few assigned them to the oxidation/reduction reactions of the Pc ring surrounding the Fe center.[25] It is surprising that such a basic but fundamentally important phenomenon still remains unclear. Moreover, the ambiguity over the redox transitions of metal macrocycles precludes rational design of these catalytic systems through optimization of their local coordinate structure.

It has become increasingly clear to us that the obscurity surrounding the redox behavior of the M−N_4 moieties is largely induced by the interaction between the active sites and electrolytes. In aqueous media, the M−N_4 center interacts with H_2O molecules or the OH_{ads} from water dissociation, which not only affects the redox potential but also alters the local structure of the M−N_4 center.[3,18] In nonaqueous media, the interaction between the M−N_4 center and the electron-donating organic solvent in the electrolyte is governed by the donor number (DN) of the solvent, as governed by the Hard Soft Acid Base (HSAB) concept.[26] The DN of a solvent is a measure of its electron-donating ability. Therefore, one plausible way to address this obscurity is to electrochemically characterize the M−N_4 catalysts in both aqueous and nonaqueous media coupled to spectroscopic techniques to elucidate the interactions between active sites, intermediates, or electrolytes to understand the redox chemistry of M−N_4 moieties and the associated catalytic activity.

In this study, we systemically investigated the redox transitions of FePc (Sigma-Aldrich) in both aqueous and nonaqueous electrolytes by combining electrochemical measurements with in situ X-ray absorption (XAS) and Raman spectroscopic analyses. The H_2Pc (Sigma-Aldrich) with the same Pc ring as FePc but without the Fe center was examined under the same conditions as a baseline material. The electrochemical features arising from the ring are expected for both moieties, whereas the features arising from the Fe-center should be absent for H_2Pc. In addition, we used in situ XAS or Raman spectra to monitor the structural and electronic changes of intact and pyrolyzed FePc/C as well as the adsorption/desorption of adsorbates over a wide range of potentials in both aqueous or nonaqueous media. We provide conclusive evidence that the redox peaks at the lower potential in aqueous media are associated with the redox behavior of the ring with the electron shuttled via the Fe(II)/Fe(I) transition of the Fe center, which is contrary to the previous interpretations of the redox behavior of FePc and the analogous metal macrocycles.

The FePc-300/C and H_2Pc/C were tested first in a 0.1 M N_2-saturated $HClO_4$ electrolyte. FePc-300/C exhibits two typical redox peaks around 0.16 V_{RHE} and 0.64 V_{RHE} (V_{RHE} represents the potential versus the reversible hydrogen electrode, RHE), whereas H_2Pc/C exhibits no features within the entire potential window (Figure 1). The difference between FePc-300/C and H_2Pc/C, which was also observed in alkaline media (Figure S1), suggests that these two redox peaks of FePc-300/C arise from the redox transition of the central Fe. If this was the case, then the redox transition would be readily captured by XAS, as the X-ray absorption near edge structure (XANES) is ultrasensitive to the electronic properties of the metal and has been used to probe the oxidation state and electronic configuration of M−N_4 moieties.[3,18,27,28] Therefore, in situ XAS was conducted on FePc-300/C at the Fe K-edge under the same condition applied for electrochemical characterizations. As seen in Figure 2a, the XANES of FePc-300/C shifts cathodically with decreasing potentials. The edge position as a function of applied potential, which reflects the oxidation state changes of Fe with potentials,[27] is summarized in Figure 2b. The shift is trivial at potentials below 0.5 V_{RHE}, and increases sharply around 0.6 V_{RHE}, which corroborates well the redox peaks around 0.64 V_{RHE} displayed in the cyclic voltammogram (CV) (Figure 1), pointing to the redox transition[18]

$$Fe(III)-OH_{ads} + H^+ + e^- \leftrightarrow Fe(II) + H_2O \quad (1)$$

It has been suggested that the surface fraction of the Fe(III) ($\Theta_{Fe(III)}$ = Fe(III)/(Fe(III) + Fe(II)) is determined by the difference between the applied potential E and the redox potential E_{redox}, as described by eq 2[29]

$$\Theta_{Fe(III)} = \frac{1}{1 + e^{-F/RT(E-E_{redox})}} \quad (2)$$

where F is the Faraday constant, R is the universal gas constant, and T is the temperature. Interestingly, the curve of $\Theta_{Fe(III)}$ derived from eq 2 with the E_{redox} of 0.64 V_{RHE} nearly overlaps the experimental $\Theta_{Fe(III)}$ of FePc-300/C derived from XANES (Figure 2b). These results firmly verify that the second redox peaks around 0.64 V indeed originate from the Fe(III)/Fe(II) redox transition, and the redox transition of Fe can be captured by in situ XAS.

However, the Fe(II)/Fe(I) redox transition previously assigned to the redox peaks at the lower potential[22−24] (Figure 1) is not seen by in situ XAS because there is no significant XANES shift around 0.16 V_{RHE} (Figure 2b). In addition, the shoulder around 7117 eV, which is the fingerprint of the square-planar Fe(II)−N_4 structure,[18,21] remains unchanged in the potential range of 0.1 to 0.5 V_{RHE}. These results indicate that the Fe(II)−N_4 configuration remains intact even below the redox potential of 0.16 V_{RHE} identified electrochemically, thereby questioning the occurrence of the Fe(II)/Fe(I) redox

DOI: 10.1021/acs.jpclett.7b01126
J. Phys. Chem. Lett. 2017, 8, 2881−2886

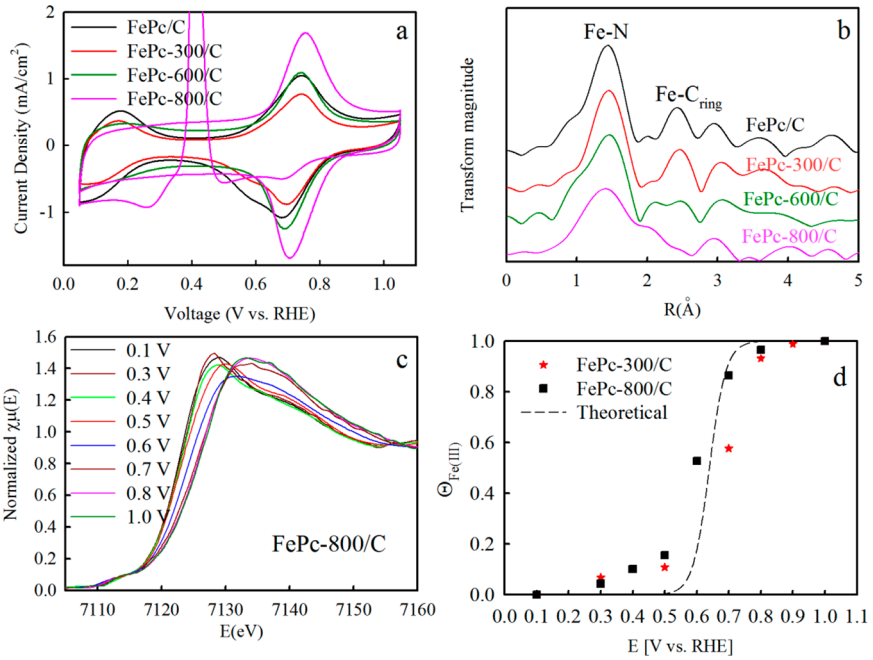

Figure 3. (a) CV plots collected for FePc/C pyrolyzed at various temperatures in a N_2-saturated 0.1 M $HClO_4$ electrolyte at 20 mVs^{-1} at room temperature; the prominent peak of FePc-800/C around 0.4 V arises from the acidic dissolution of the iron oxides formed upon high-temperature treatment, as we discussed previously.[21] (b) FT-EXAFS of FePc/C pyrolyzed at various temperatures. (c) In situ XANES of FePc-800/C collected at 0.1 to 1.0 V_{RHE} in N_2-saturated 0.1 M $HClO_4$ at room temperature. (d) Experimental $\Theta_{Fe(III)}$ for FePc-300/C and FePc-800/C in comparison with the calculated $\Theta_{Fe(III)}$ derived from eq 2.

transition. To ensure that the imperceptibility of the Fe(II)/Fe(I) redox transition to in situ XAS is not related to the low potential region or acidic media, iron tetraphenylporphyrin (FeTPP) pyrolyzed at 300 °C was chosen for similar studies in 0.1 M KOH, in which its Fe(III)/Fe(II) redox potential is ~0.3 V_{RHE} (Figure S2a). This redox transition can be captured by in situ XAS, as reflected by the XANES shift with potentials (Figure S2b).

Because the in situ XAS results implicate that the redox peaks of FePc around 0.16 V_{RHE} is not associated with the Fe(II)/Fe(I) redox transition, we examined the alternative explanation that relates the redox peaks to the redox behavior of the Pc ring. We pyrolyzed FePc/C at various temperatures, which has been demonstrated to selectively demolish the ring but preserve the Fe−N_4 center.[18,21,30] As a result, the redox peaks around 0.64 V_{RHE} associated with the Fe(III)/Fe(II) redox transition are present in the CVs of all pyrolyzed FePc/C samples (Figure 3a), indicating the preservation of the Fe−N_4 center. This is further confirmed by the XANES shift of the FePc/C pyrolyzed at 800 °C (FePc-800/C), with potentials that closely resemble that of FePc-300/C (Figure 3c,d). Conversely, the redox peaks around 0.16 V_{RHE} gradually diminish with increasing pyrolysis temperature, suggesting the destruction of the Pc ring. This was also confirmed by the disappearance of the Fourier transform of the extended X-ray absorption fine structure (EXAFS) signals around 2.5 Å arising from the scattering of the second shell of the carbon atoms in the Pc ring (Figure 3b). The observation that the destruction of the ring of FePc is accompanied by the disappearance of the redox peaks around 0.16 V_{RHE} strongly suggests that the redox peaks of FePc around 0.16 V_{RHE} arise from the redox behavior of the Pc ring rather than the Fe(II)/Fe(I) redox transition, as widely assumed hitherto. This argument is further supported by the observation that the Fe−N_4 materials synthesized NOT from metal macrocycle precursors with pre-existing Fe−N_4 moiety only exhibit the Fe(III)/Fe(II) redox peaks at the high potential.[1,18] However, the assignment of the low potential redox peaks to the Pc ring seemingly contradicts the absence of the redox peaks for H_2Pc that also contains the Pc ring.

Note that the absence of either the metal center (H_2Pc) or the ring (FePc-800/C) leads to the absence of the redox peaks at the low potential end. This implicates that this redox transition probably involves both the metal center and the ring. The imperceptibility of the Fe(II)/Fe(I) redox transition to in situ XAS does not necessarily mean that this transition does not happen. An oxidation state of Fe needs to be stable to be captured by XAS. This is unlikely the case for all three oxidation states of iron involved here. The Fe(II)Pc (with its electronic configuration of $[Ar]4s^23d^6$) in the neat state or in aqueous media is at the intermediate spin state,[3] which is a stable state as the fully occupied d_z^2 orbital inhibits the charge transfer from the axial ligand to the d_z^2 orbital. The Fe(II)Pc can switch to the low spin state in nonaqueous media upon complexation with axial ligands, and this octahedral complex is stable as the Fe has fully occupied t_{2g} orbitals with all the d-electrons paired.[13] The Fe(III) state ($[Ar]4s^23d^5$) with an unpaired t_{2g} electron is stabilized by the axial adsorption of OH^- from water splitting (eq 1). The Fe(I) state ($[Ar]4s^23d^7$) also contains an unpaired e_g electron and requires a strongly electron-donating axial ligand for stabilization, which may not occur in aqueous media due to the lack of a suitable axial ligand. If this was the case, then the Fe(I) state would be invisible to XAS despite the occurrence of the Fe(II)/Fe(I) redox transition.

To test the hypothesis, FePc and H_2Pc/C were studied in a high DN organic solvent dimethyl sulfoxide (DMSO)-based electrolyte, anticipating that the strong interaction between the Fe−N_4 center and the DMSO with its DN of 29.8 may stabilize

DOI: 10.1021/acs.jpclett.7b01126
J. Phys. Chem. Lett. 2017, 8, 2881−2886

the Fe(I) state. As seen in Figure 4, FePc exhibits three redox peaks at 2.2, 2.6, and 3.8 V (the potentials in nonaqueous media are versus Li/Li^+ reference electrode), respectively, whereas the H_2Pc/C exhibits a couple of prominent peaks around 2.3 V, followed by a couple of trivial peaks around 2.6 V. The small peaks of H_2Pc/C around 2.6 V arise from the FePc impurities in the commercial H_2Pc/C.[31] The peaks at 2.2 and 2.3 V are from the ring for FePc/C and H_2Pc/C, respectively. The slight difference in their redox potentials is expected from the interaction between the Fe−N_4 center and the ring that alters the electronic properties of the ring. These comparison results indicate that the redox peaks around 2.6 V arise from the Fe(II)/Fe(I) redox transition. This is further verified by in situ Raman (in situ XAS is not suitably applicable to this nonaqueous electrolyte system owing to technological limitations associated with a volatile solvent in a flowing O_2 atmosphere), as shown next.

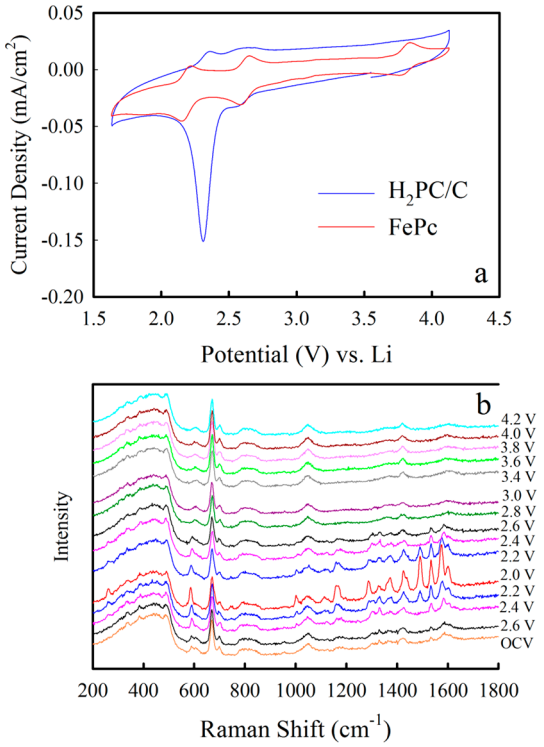

Figure 4. (a) CVs of H_2Pc/C on a glassy carbon electrode in an Ar-purged solution of 0.1 M $LiPF_6$/DMSO and 1 mM FePc dissolved in the same Ar-purged electrolyte with a scan rate of 10 mV s^{-1}. (b) In situ Raman spectra recorded for Ar-purged 1 mM FePc/0.1 M $LiPF_6$ in DMSO.

In situ Raman spectra were collected as the electrode was scanned cathodically from the open-circuit voltage (OCV = 2.74 V) to 2.0 V and then scanned anodically to 4.0 V to capture the redox transitions of FePc (Figure 4). Reversible Raman peaks at 260, 584, 745, and 1000 cm^{-1} and between 1000 and 1600 cm^{-1} were observed when the electrode potential was scanned across 2.6 V. To facilitate the interpretation of these occurrences, the changes of the local coordinates and structure of FePc upon the redox-induced interactions with DMSO are depicted in Scheme 1. At the OCV, the FePc is in the Fe(II) state and six-coordinated containing two DMSO molecules at the axial positions, $(DMSO)_2Fe(II)Pc$.[32] The appearance of the Raman peaks below 2.6 V indicates the symmetry change associated with the loss of the planarity of $(DMSO)_2Fe(II)Pc$ upon the formation of an asymmetric five-coordinated complex (DMSO)Fe(I)Pc by releasing one of the two DMSO molecules.[13,33] When Fe(I)Pc was further reduced as the electrode was polarized down to 2.0 V, the Pc ring was reduced as reflected by the new Raman peaks at 1425 and 1490 cm^{-1} (Figure 4) that can be assigned to the pyrrole C−C and C−N stretching vibrations arising from the reduction of the ring (Scheme 1).[13,33] These results verify the redox transition of the Fe(II)/Fe(I) as well as of the ring of FePc in nonaqueous media.

Because the redox transitions of Fe(III)/Fe(II) and the ring were detected by spectroscopy both in aqueous and nonaqueous media, we infer that the Fe(II)/Fe(I) redox transition observed in nonaqueous media also occurs in aqueous electrolytes but just indiscernible to spectroscopy, especially considering that the redox behavior is determined by the nature of the active center. The major difference between nonaqueous media and aqueous media is that in the former environment the solvent (DMSO here) can stabilize the Fe(I) state by coupling with the unpaired $3d_{z^2}$ (e_g^1) electron via the formation of (DMSO)Fe(I)Pc with DMSO bound to the axial position;

Scheme 1. Redox Behaviors of the FePc in Nonaqueous (left) and Aqueous Media (right)

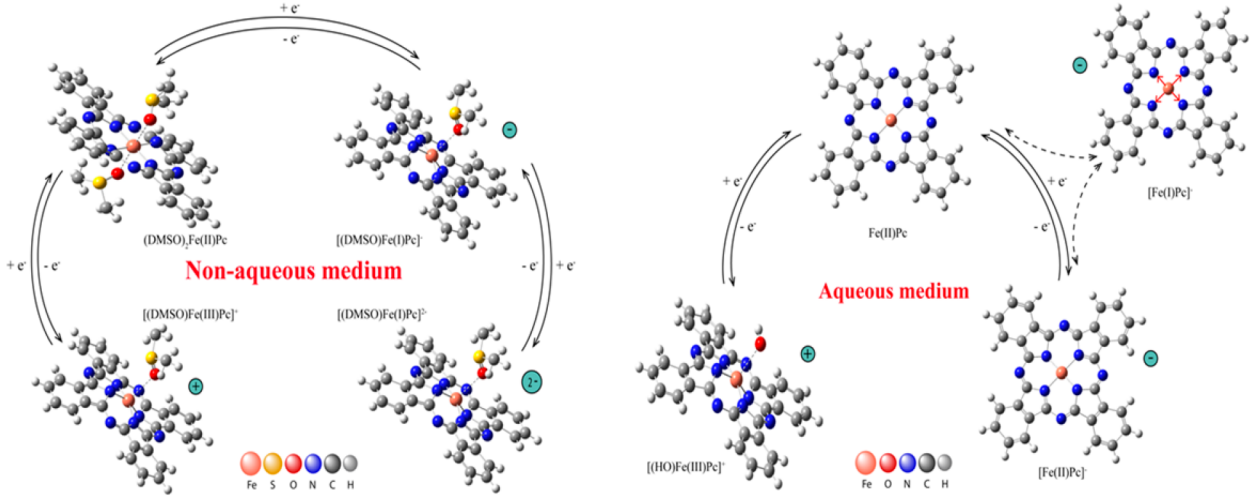

DOI: 10.1021/acs.jpclett.7b01126
J. Phys. Chem. Lett. 2017, 8, 2881−2886

whereas the Fe(I) state is not stabilized in aqueous media due probably to the low donor number of water (DN = 18) (Scheme 1), which is not a strong enough electron donor to bind with the e_g^1 electron. As a result, the unpaired e_g electron is spontaneously delocalized into an empty π^* orbital of the Pc ring forming $[Fe(II)Pc]^-$.[25,34] In other words, the Fe(II)/Fe(I) redox transition of FePc still occurs in aqueous media despite its imperceptibility, but the redox peaks are formally associated with the redox of the Pc ring with the electron shuttled via the Fe(II)/Fe(I) redox transition of the Fe center. This delicate picture highlights the critical role of the metal center in promoting the redox behavior of the macrocycle ring. It provides a plausible explanation for the redox peaks of FePc at the low potential end requiring the presence of both the metal center and the macrocycle ring.

In summary, we have demonstrated that the redox peaks of FePc at the low potential end in aqueous media are associated with neither solely the Fe(II)/Fe(I) redox transition nor solely the redox behavior of the ring, as previously assumed. They are associated with the redox behavior of the ring with the electron shuttled to it via the Fe(II)/Fe(I) redox transition of the Fe center, which is indiscernible by means of regular spectroscopy methods owing to the lack of a suitable axial ligand to stabilize the Fe(I) state. This fundamental knowledge to electrocatalysis resolves the long-held ambiguity about the redox transitions of metal macrocycles in ORR catalysis.

■ ASSOCIATED CONTENT

Supporting Information

The Supporting Information is available free of charge on the ACS Publications website at DOI: 10.1021/acs.jpclett.7b01126.

Description of the material included. Experimental details and supporting figures, including the CVs and the in situ XANES of FeTPP-300/C. (PDF)

■ AUTHOR INFORMATION

Corresponding Author

*E-mail: q.jia@neu.edu.

ORCID

Jingkun Li: 0000-0003-1699-3089

Sanjeev Mukerjee: 0000-0002-2980-7655

Qingying Jia: 0000-0002-4005-8894

Present Address

§N.R.: Global Fuel Cell Activities, General Motors Corporation, Pontiac, MI 48340, United States.

Notes

The authors declare no competing financial interest.

■ ACKNOWLEDGMENTS

Financial support from U.S. Army Cerdec via subcontract no. GTS-S-15-015 is gratefully acknowledged. A scholarship for A.A. by King Abdulaziz University and the Saudi Arabian Cultural Mission is appreciated. Use of the synchrotron facilities at the National Synchrotron Light Source (NSLS), beamlines X19A at Brookhaven National Laboratory (BNL), Upton, NY is supported by the U.S. Department of Energy, Office of Science, Office of Basic Energy Sciences, formerly under contract no. DE-AC02-98CH10886. Use of the Stanford Synchrotron Radiation Lightsource, SLAC National Accelerator Laboratory, is supported by the U.S. Department of Energy, Office of Science, Office of Basic Energy Sciences under contract no. DE-AC02-76SF00515. Use of Beamline 2-2 at SSRL was partially supported by the NSLS-II, BNL, under U.S. Department of Energy contract no. DE-SC0012704. Support from beamline personnel Dr. Syed Khalid and Dr. Nebojsa Marinkovic is gratefully appreciated.

■ REFERENCES

(1) Wu, G.; More, K. L.; Johnston, C. M.; Zelenay, P. High-performance electrocatalysts for oxygen reduction derived from polyaniline, iron, and cobalt. *Science* **2011**, *332*, 443−447.

(2) Lefèvre, M.; Proietti, E.; Jaouen, F.; Dodelet, J.-P. Iron-based catalysts with improved oxygen reduction activity in polymer electrolyte fuel cells. *Science* **2009**, *324*, 71−74.

(3) Li, J.; Ghoshal, S.; Liang, W.; Sougrati, M.-T.; Jaouen, F.; Halevi, B.; McKinney, S.; McCool, G.; Ma, C.; Yuan, X.; et al. Structural and mechanistic basis for the high activity of Fe−N−C catalysts toward oxygen reduction. *Energy Environ. Sci.* **2016**, *9*, 2418−2432.

(4) Zitolo, A.; Goellner, V.; Armel, V.; Sougrati, M.-T.; Mineva, T.; Stievano, L.; Fonda, E.; Jaouen, F. Identification of catalytic sites for oxygen reduction in iron-and nitrogen-doped graphene materials. *Nat. Mater.* **2015**, *14*, 937−942.

(5) Wei, P. J.; Yu, G. Q.; Naruta, Y.; Liu, J. G. Covalent grafting of carbon nanotubes with a biomimetic heme model compound to enhance oxygen reduction reactions. *Angew. Chem., Int. Ed.* **2014**, *53*, 6659−6663.

(6) Cao, R.; Thapa, R.; Kim, H.; Xu, X.; Kim, M. G.; Li, Q.; Park, N.; Liu, M.; Cho, J. Promotion of oxygen reduction by a bio-inspired tethered iron phthalocyanine carbon nanotube-based catalyst. *Nat. Commun.* **2013**, *4*, 2076.

(7) Zhang, Z.; Gao, X.; Dou, M.; Ji, J.; Wang, F. Fe-Nx moiety-modified hierarchically porous carbons derived from porphyra for highly effective oxygen reduction reaction. *J. Mater. Chem. A* **2017**, *5*, 1526−1532.

(8) Yuan, X.; Zeng, X.; Zhang, H.-J.; Ma, Z.-F.; Wang, C.-Y. Improved performance of proton exchange membrane fuel cells with p-toluenesulfonic acid-doped Co-PPy/C as cathode Electrocatalyst. *J. Am. Chem. Soc.* **2010**, *132*, 1754−1755.

(9) Tolmachev, Y. V.; Vorotyntsev, M. A. Fuel cells with chemically regenerative redox cathodes (review). *Russ. J. Electrochem.* **2014**, *50*, 403−411.

(10) Li, L.; Yuan, X.; Ma, Z.; Ma, Z.-F. Properties of pyrolyzed carbon-supported cobalt-polypyrrole as electrocatalyst toward oxygen reduction reaction in alkaline media. *J. Electrochem. Soc.* **2015**, *162*, F359−F365.

(11) Shui, J.-L.; Karan, N. K.; Balasubramanian, M.; Li, S.-Y.; Liu, D.-J. Fe/N/C composite in Li−O_2 battery: studies of catalytic structure and activity toward oxygen evolution reaction. *J. Am. Chem. Soc.* **2012**, *134*, 16654−16661.

(12) Trahan, M. J.; Jia, Q.; Mukerjee, S.; Plichta, E. J.; Hendrickson, M. A.; Abraham, K. M. Cobalt phthalocyanine catalyzed lithium-air batteries. *J. Electrochem. Soc.* **2013**, *160*, A1577−A1586.

(13) Gunasekara, I.; Ates, M. N.; Mukerjee, S.; Plichta, E. J.; Hendrickson, M. A.; Abraham, K. Solid phase FePC catalysts for increased stability of oxygen reduction reaction intermediates at the cathode/electrolyte interface in lithium air batteries. *J. Electrochem. Soc.* **2017**, *164*, A760−A769.

(14) Auwärter, W.; Écija, D.; Klappenberger, F.; Barth, J. V. Porphyrins at interfaces. *Nat. Chem.* **2015**, *7*, 105−120.

(15) Yuan, X.; Li, L.; Ma, Z.; Yu, X.; Wen, X.; Ma, Z.-F.; Zhang, L.; Wilkinson, D. P.; Zhang, J. Novel nanowire-structured polypyrrole-cobalt composite as efficient catalyst for oxygen reduction reaction. *Sci. Rep.* **2016**, *6*, 20005.

(16) Zhang, Z.; Dou, M.; Ji, J.; Wang, F. Phthalocyanine tethered iron phthalocyanine on graphitized carbon black as superior electrocatalyst for oxygen reduction reaction. *Nano Energy* **2017**, *34*, 338−343.

(17) Zagal, J. H.; Koper, M. Reactivity descriptors for the activity of molecular MN_4 catalysts for the oxygen reduction reaction. *Angew. Chem., Int. Ed.* **2016**, *55*, 14510−14521.
(18) Jia, Q.; Ramaswamy, N.; Hafiz, H.; Tylus, U.; Strickland, K.; Wu, G.; Barbiellini, B.; Bansil, A.; Holby, E. F.; Zelenay, P.; et al. Experimental observation of redox-induced Fe−N switching behavior as a determinant role for oxygen reduction activity. *ACS Nano* **2015**, *9*, 12496−12505.
(19) Li, J.; Alsudairi, A.; Ma, Z.-F.; Mukerjee, S.; Jia, Q. Asymmetric volcano trend in oxygen reduction activity of Pt and non-Pt catalysts: in situ identification of the site-blocking effect. *J. Am. Chem. Soc.* **2017**, *139*, 1384−1387.
(20) Zagal, J. H.; Gulppi, M.; Isaacs, M.; Cárdenas-Jirón, G.; Aguirre, M. J. s. Linear versus volcano correlations between electrocatalytic activity and redox and electronic properties of metallophthalocyanines. *Electrochim. Acta* **1998**, *44*, 1349−1357.
(21) Ramaswamy, N.; Tylus, U.; Jia, Q.; Mukerjee, S. Activity descriptor identification for oxygen reduction on nonprecious electrocatalysts: linking surface science to coordination chemistry. *J. Am. Chem. Soc.* **2013**, *135*, 15443−15449.
(22) Baranton, S.; Coutanceau, C.; Garnier, E.; Léger, J.-M. How does α-FePc catalysts dispersed onto high specific surface carbon support work towards oxygen reduction reaction (orr)? *J. Electroanal. Chem.* **2006**, *590*, 100−110.
(23) Zagal, J.; Paez, M.; Tanaka, A.; Dos Santos, J.; Linkous, C. Electrocatalytic activity of metal phthalocyanines for oxygen reduction. *J. Electroanal. Chem.* **1992**, *339*, 13−30.
(24) Bett, J. S.; Kunz, H. R.; Aldykiewicz, A. J., Jr; Fenton, J. M.; Bailey, W. F.; McGrath, D. V. Platinum-macrocycle co-catalysts for the electrochemical oxidation of methanol. *Electrochim. Acta* **1998**, *43*, 3645−3655.
(25) Ha, S. Y.; Park, J.; Ohta, T.; Kwag, G.; Kima, S. In situ iron k-edge XANES study of iron phthalocyanine irreversibly adsorbed on an electrode surface. *Electrochem. Solid-State Lett.* **1999**, *2*, 461−464.
(26) Trahan, M. J.; Gunasekara, I.; Mukerjee, S.; Plichta, E. J.; Hendrickson, M. A.; Abraham, K. Solvent-coupled catalysis of the oxygen electrode reactions in lithium-air batteries. *J. Electrochem. Soc.* **2014**, *161*, A1706−A1715.
(27) Bae, I. T.; Tryk, D. A.; Scherson, D. A. Effect of heat treatment on the redox properties of iron porphyrins adsorbed on high area carbon in acid electrolytes: an in situ Fe k-edge x-ray absorption near-edge structure study. *J. Phys. Chem. B* **1998**, *102*, 4114−4117.
(28) Zhang, H.-J.; Yuan, X.; Ma, Z.-F.; Wen, W.; Yang, J. Investigation of non-precious metal CoN_4-based oxygen reduction catalyst by electrochemical and x-ray absorption spectroscopy techniques. *J. Electrochem. Soc.* **2014**, *161*, H155−H160.
(29) Gottesfeld, S. Generation of active sites by potential-driven surface processes: a central aspect of electrocatalysis. *ECS Trans.* **2014**, *61*, 1−13.
(30) Bouwkamp-Wijnoltz, A.; Visscher, W.; Van Veen, J.; Boellaard, E.; Van der Kraan, A.; Tang, S. On active-site heterogeneity in pyrolyzed carbon-supported iron porphyrin catalysts for the electrochemical reduction of oxygen: an in situ mössbauer study. *J. Phys. Chem. B* **2002**, *106*, 12993−13001.
(31) Sawaki, Y.; Ogata, Y. Mechanism of the reaction of nitriles with alkaline hydrogen peroxide. Reactivity of peroxycarboximidic acid and application to superoxide ion reaction. *Bull. Chem. Soc. Jpn.* **1981**, *54*, 793−799.
(32) Jones, J. G.; Twigg, M. Axial ligand exchange reactions of ferrous phthalocyanine. Exchange of imidazole for dimethyl sulfoxide. *Inorg. Chem.* **1969**, *8*, 2120−2123.
(33) Liu, Z.; Zhang, X.; Zhang, Y.; Jiang, J. Theoretical investigation of the molecular, electronic structures and vibrational spectra of a series of first transition metal phthalocyanines. *Spectrochim. Acta, Part A* **2007**, *67*, 1232−1246.
(34) Fierro, C.; Anderson, A. B.; Scherson, D. A. Electron donor-acceptor properties of porphyrins, phthalocyanines, and related ring chelates: a molecular orbital approach. *J. Phys. Chem.* **1988**, *92*, 6902−6907.

DOI: 10.1021/acs.jpclett.7b01126
J. Phys. Chem. Lett. 2017, 8, 2881−2886